Tectonophysics 893 (2024) 230541

Contents lists available at ScienceDirect

Tectonophysics

journal homepage: www.elsevier.com/locate/tecto

Present-day incipient fault coalescence at a relay zone (Jiloca extensional basin, Spain): Evidence from instrumental seismicity

Alba Peiro [a], Lucía Lozano [b,d], Luis E. Arlegui [c], Juan V. Cantavella [d], Sandra Ruiz-Barajas [d], José L. Simón [c,*]

[a] Fundación Ibercivis, Edificio I+D-Campus Río Ebro, C/ Mariano Esquillor s/n, 50018 Zaragoza, Spain
[b] Dpto. de Física de la Tierra y Astrofísica, Universidad Complutense de Madrid, 28040 Madrid, Spain
[c] Dpto. de Ciencias de la Tierra, Grupo Geotransfer - Instituto Universitario de Investigación en Ciencias Ambientales de Aragón (IUCA), Universidad de Zaragoza, Pedro Cerbuna 12, 50009 Zaragoza, Spain
[d] Red Sísmica Nacional, Instituto Geográfico Nacional (IGN), Ibáñez de Ibero, 3, 28003 Madrid, Spain

ARTICLE INFO

Keywords:
Fault linkage
Intraplate seismotectonics
Present-day stress field
Jiloca graben

ABSTRACT

The relay zones between NW-SE to NNW-SSE striking faults of the Jiloca graben (Iberian Chain) mostly show distributed along-strike fault and fracture patterns. The latter are chiefly controlled by the Late Pliocene-Quaternary regional stress field, and secondarily respond to local controls from inherited structures. Such fracture patterns contrast with the classical models of transverse connecting faults controlled by relay kinematics. North of the Concud fault trace, at the relay zone with the Sierra Palomera fault, an unusually high seismic activity has been noticed since 2014, with magnitudes up to M = 3.5. Upgrading of the National Seismic Network allowed obtaining such new detailed records, while the installation of a new seismometer by the IGN within the study area has improved the reliability of focal depth data since 2017. A high-precision absolute relocation of seismicity from 01/01/2000 to 30/05/2022 has been carried out. The results show that (i) the epicentres are significantly clustered along a nearly N-S trending band, and (ii) the focal depths range from 0 to 14 km, in good agreement with the thickness of the brittle crust. This 3D spatial distribution of seismicity is interpreted as a consequence of activation of either a single fault or a fault zone, nearly vertical and N-S striking. Such structural setting is consistent with the surficial fracture patterns observed at both map and outcrop scale: NNW-SSE and NNE-SSW oriented faults and fractures, orthogonal to the ENE-WSW to ESE-WNW regional σ_3 trajectories, together with NW-SE trending ones controlled by inherited contractive faults. The present-day seismic activity suggests that along-strike, incipient fault propagation at the relay zone between the Concud and Sierra Palomera faults is currently operating under the control of the remote stress field.

1. Introduction

Models of extensional fault linkage have been extensively developed during the last decades. Numerical and analogue modelling, as well as natural examples, have increased our understanding on the role of the main controls of fault interaction and propagation in fault relay zones: structural inheritance, relay kinematics, remote stress field (e.g., Peacock and Sanderson, 1991, 1994; Willemse, 1997; Crider and Pollard, 1998; Mansfield and Cartwright, 2001; Peiro et al., 2020; see particularly the reviews by Peacock, 2002, and Fossen and Rotevatn, 2016). The conceptual model of *soft linkage* (relay ramp) evolving to *hard linkage* (breached ramp) would result in transverse connecting fractures, at high angles to the master faults. This model has been extensively represented in published sketches (e.g., Ramsay and Huber, 1987, p. 533; Peacock, 2002, Fig. 3c; Fossen and Rotevatn, 2016), but much less described in actual cases (e.g. Peacock and Sanderson, 1994, Figs. 2, 14, 15). Examples of fracture patterns (including faults and joints) at low angles to the major faults seem to be more frequent indeed, either in the form of longitudinal, along-strike faults propagated from a major fault tip (e.g., Childs et al., 1995; Walsh et al., 1999, Figs. 3d, 5a; Fossen and Rotevatn, 2016, Fig. 6), or longitudinal distributed fracture patterns, frequently including both synthetic and antithetic faults (e.g., Peacock

* Corresponding author.
E-mail addresses: apeiro@ibercivis.es (A. Peiro), lllopezdemedrano@transportes.gob.es (L. Lozano), arlegui@unizar.es (L.E. Arlegui), jvcantavella@transportes.gob.es (J.V. Cantavella), srbarajas@transportes.gob.es (S. Ruiz-Barajas), jsimon@unizar.es (J.L. Simón).

https://doi.org/10.1016/j.tecto.2024.230541
Received 12 July 2024; Received in revised form 16 October 2024; Accepted 20 October 2024
Available online 22 October 2024

and Sanderson, 1994, Figs. 4a, 9a; Anders and Schlische, 1994, Fig. 3b; Trudgill and Cartwright, 1994, Figs. 3b,5,6; Mansfield and Cartwright, 2001, Fig. 7).

Based on both analogue models and field examples, Peiro et al. (2020) stated that fracture propagation in extensional fault relay zones may not be chiefly controlled by 'internal' kinematics (elongation along the relay ramp), but determined by 'external' controls. The authors proposed a new conceptual model of fault coalescence guided by distributed along-strike propagated fractures (Fig. 1), most of them externally controlled (either parallel to the inherited structural trends, or responding to the remote stress field) instead of being internally induced by the own relay kinematics.

One of the examples studied by Peiro et al. (2020), and used as field reference for their model, is the relay zone between the Concud and Sierra Palomera faults, at the eastern boundary of the Jiloca graben. This active graben is located in the central-eastern Iberian Chain, Spain (Fig. 2), a region considered to be of low seismic hazard, but exhibiting a number of large faults active during Late Pleistocene-Holocene times.

At the wide relay zone between the Concud and Sierra Palomera faults (Fig. 2), an unusually high seismic activity has been noticed since 2014, coinciding with upgrading of the Spanish National Seismic Network of Instituto Geográfico Nacional (IGN). Such abnormal seismicity mostly occurs north of the Concud fault, an extensional fault whose structure and paleoseismicity had been intensively studied in previous years (Lafuente, 2011; Lafuente et al., 2011a, 2014; Simón et al., 2012, 2016). The study of such seismic activity opens the possibility of comparing the present-day tectonic setting revealed by instrumental earthquakes with the Late Pleistocene slip history of that fault.

With this view, an attempt was made to increase the low seismic station density of this area, and hence to expand and improve its seismic record, by installing a new seismometer. IGN installed a portable seismometer in 2017 at a site near Celadas village (north of the Concud fault), which has rendered a 5-year continuous seismic record that has included a large number of micro-earthquakes not detected by the National Seismic Network. After being analysed and filtered, such seismic information could provide new insights into the evolutionary model of fault relay evolution proposed by Peiro et al. (2020).

Fault propagation patterns are key for assessing seismogenic potential of fault zones, since they determine the effective area of coseismic rupture for a given fault or fault segment. In some cases, bands of seismicity reveal the occurrence of blind, previously unrecognized faults lacking a surface expression, which contributes to the knowledge of present-day processes of fault propagation. Bawden et al. (1999) described a noteworthy example in California, close to the Big Bend

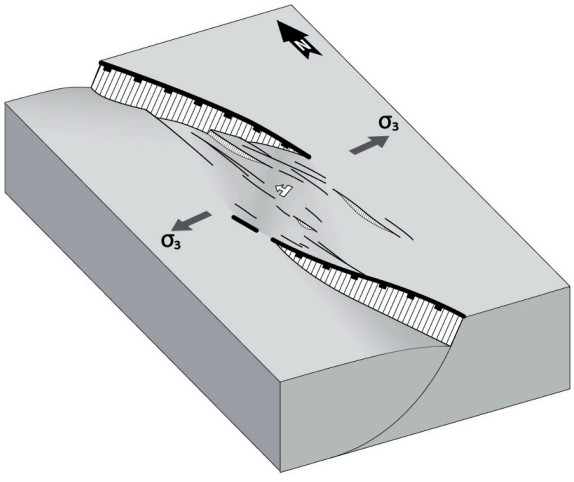

Fig. 1. 3D conceptual model of a relay zone with distributed, along-strike propagated fractures that accommodate the double influence of structural heritage and remote stress field (after Peiro et al., 2020).

segment of the San Andreas fault. An elongated cluster of earthquakes define a NE-SW trending lineament that was interpreted as an incipient propagation of the White Wolf fault towards the northeast. Other similar cases have been reported more recently by Lai et al. (2009) in NE Taiwan, Lieser et al. (2014) in central Chile, Bonini et al. (2016) in northern Apennines, Ferrarini et al. (2021) in central Apennines, or Koirala et al. (2023) in Nepalese Himalaya.

Propagation and eventual coalescence of neighbouring faults in the Teruel-Jiloca region have been object of debate, mostly concerning the narrow (1.3 km wide) relay zone between the Concud and Teruel faults (Fig. 2b). It was suggested (Gutiérrez et al., 2012) that both make a single seismogenic structure, therefore involving the possibility of larger earthquakes than those generated by each separate structure. Macro- and mesostructural data indicate that they are independent structures from the geometrical and kinematical point of view (Lafuente, 2011; Lafuente et al., 2011b), but displacement gradients close to the relay zone suggest that both faults undergo dynamic interaction and are at a transient stage to linkage (Simón et al., 2017). Given the prevalence of recent NNW-SSE trending fractures within the relay zone, controlled by the ENE-WSW trending σ_3 trajectories of the remote stress field, such future coalescence will be probably achieved by progressive propagation of along-strike fractures (Peiro et al., 2017, 2020). In the case of the relay zone between the Concud and Sierra Palomera faults, the long distance between their map traces would initially suggest that they are still a long way off from coalescing, but the new seismic information can provide clues to understanding their definite present-day tectonic setting.

The objectives of the present work are:

1) Synthesizing and refining previous information on fault patterns in the relay zone between the Concud and Sierra Palomera fualts.
2) Compiling seismic data provided by the National Seismic Network for the study area, as well as those delivered by the new seismometer of Celadas.
3) Evaluating the seismic record available for the study area; in particular, its completeness and the improvement due to the new seismic station of Celadas.
4) Analysing the temporal distribution of seismicity during the last two decades in order to know whether the increase in activity since 2014 is real or apparent.
5) Characterizing the 3D distribution of seismic foci by means of a non-linear probabilistic relocation of the seismicity for the whole period, and hence inferring present-day fault patterns in the Concud-Sierra Palomera relay zone.
6) Comparing such present-day fault patterns with those observed in recent fracturing, and evaluating their consistence with the regional stress field.
7) Testing the validity of the evolutionary model of fault relay zones with distributed longitudinal fractures (Peiro et al., 2020).

2. Geological and seismological setting

The intraplate Iberian Chain is a NW-SE trending mountain chain located within the Iberian Peninsula (Fig. 2a), which developed during the Cenozoic under the convergence with both the European and African plates (Álvaro et al., 1979; Capote et al., 2002). Its macrostructure mainly consists in NW-SE (locally *E*-W) trending fold-and-thrust belts resulting from inversion of Mesozoic basins (Liesa et al., 2018) during compressional episodes of the Alpine Orogeny (Paleogene to early Neogene; Liesa and Simón, 2009).

The eastern Iberian Chain shows a large network of Neogene-Quaternary extensional basins that postdate and obliquely cut the contractional structures (Fig. 2a). They represent the onshore extensional system linked to rifting of the Valencia Trough, which evolved through two episodes: (i) during the Late Miocene-Early Pliocene, NNE-SSW trending grabens (Teruel and Maestrat, parallel to the Valencia

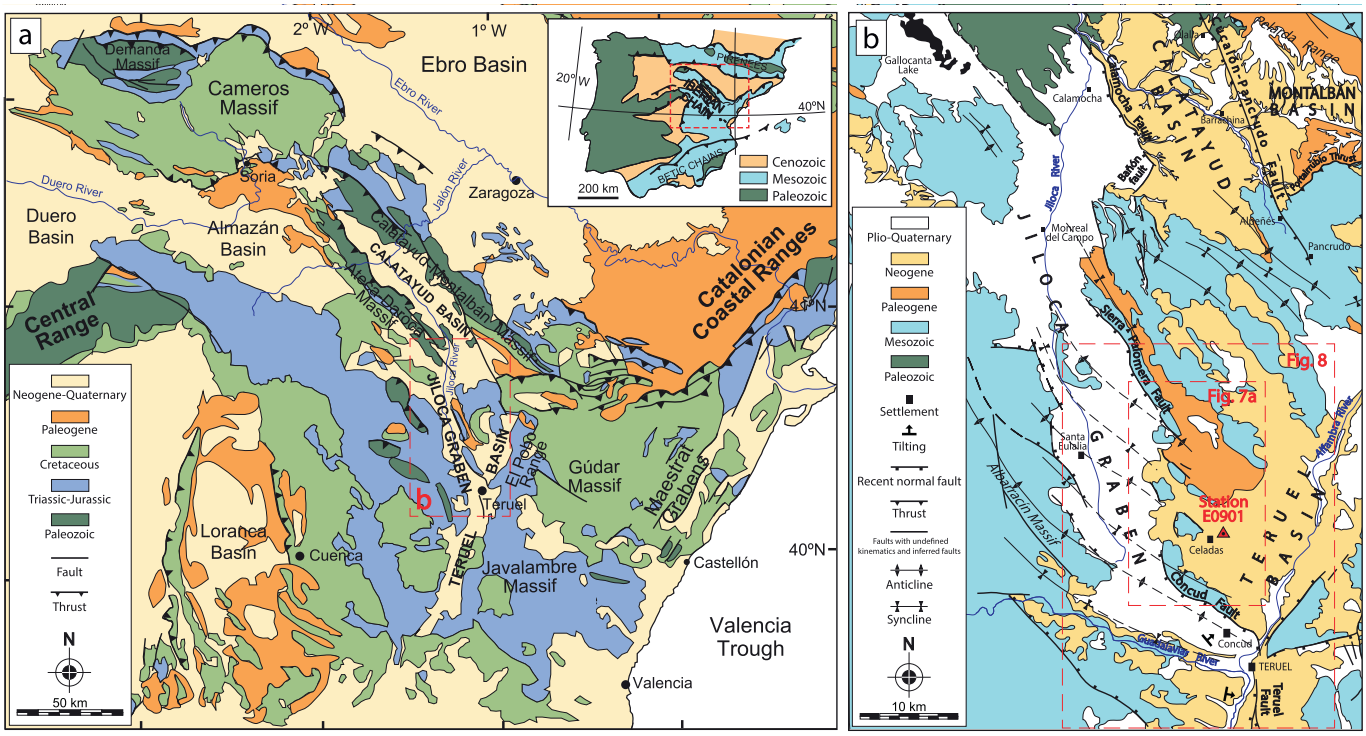

Fig. 2. (a) Simplified geological map of the Iberian Chain (inset: location within the Iberian Peninsula). (b) Jiloca fault system, with the relay zones between the Concud, Sierra Palomera and Calamocha faults.

Trough) developed under an extensional stress field with WNW-ESE trending σ_3 trajectories; (ii) during the Late Pliocene-Quaternary, reactivation of the former basins and onset of the new NNW-SSE trending Jiloca graben took place, under radial or multidirectional extension (σ_1 vertical, $\sigma_2 \approx \sigma_3$) with σ_3 usually trending WSW-ENE (occasionally, E-W to ESE-WSW) (Simón, 1982, 1983, 1989; Arlegui et al., 2005; Liesa et al., 2019; Simón et al., 2022). This stress field has essentially remained up to the present-day (Herraiz et al., 2000). In any case.

The Jiloca graben shows an overall NNW-SSE trend that results from an en-échelon right-releasing arrangement of NW-SE-striking, nearly pure normal faults, the main ones being located at the eastern boundary: Calamocha, Sierra Palomera and Concud faults (Fig. 2b). The Sierra Palomera fault bounds the central sector of the Jiloca graben, accommodating a throw of 480 m during the last 3.8 Ma. A minor antithetic fault, induced by rollover bending associated to it, shows evidence of activity during Late Pleistocene time (Peiro et al., 2022). The Concud fault, separated from the former one by a wide relay zone, shows overall NW–SE strike that veers towards NNW–SSE near its southern and northern tips. The accumulated net slip since 3.5 Ma is estimated within the range of 255–290 m (long-term slip rate = 0.07–0.08 mm/a), while paleoseismological studies reveal recurrent and faster movement during the Late Pleistocene (at least eleven events since ca. 74 ka; net slip rate of 0.29 mm/a; Lafuente et al., 2011a, Lafuente et al., 2014; Simón et al., 2016).

The relay zone between the Concud and Sierra Palomera faults takes de form of a gentle, irregular relay ramp articulated by a number of shorter, disconnected faults (Fig. 2b). It is an underlapping relay zone (the traces of the two master faults are far from overlapping indeed), with their tips being about 12 km apart (overlapping length = −9.5 km; virtual width ~ 7 km). Jurassic and Paleogene materials crop out in the zone, unconformably covered by Neogene (Upper Miocene to Upper Pliocene) units mostly made of alluvial lutites and lacustrine carbonates. Such Neogene units belong to the neighbouring Teruel basin, and are probably connected through this relay zone with the lower infill (not exposed) of the Jiloca basin (Rubio and Simón, 2007).

Located southwards of the Concud fault and separated by a narrow (less than 1 km) relay zone, the Teruel fault is a N-S striking, intrabasinal fault that offsets the Neogene infill of the Teruel basin (Fig. 2b). It accommodates net slip of ca. 270 m since ~3.5 Ma, and shows significant Late Pleistocene activity, with at least four events occurring between 76.0 and 9.2 ka (Simón et al., 2017).

The low long-term (Plio-Pleistocene) slip rates computed for the main faults all along the Central-eastern Iberian Chain (in the range of 0.05 to 0.15 mm/a; average: 0.08 mm/a; Simón et al., 2022), even the short-term (Late Pleistocene) slip rates (in the range of 0,05–0,36 mm/a; average: 0,21 mm/a), suggest a low regional strain rate. Unfortunately, we have no GPS data available for quantifying it in the present day.

Historic and instrumental seismicity of the region is low to moderate (see Fig. 3). The epicentres are concentrated along N-S striking faults of the southern Teruel basin, the western margin of the Jiloca basin, and the Albarracín and Javalambre massifs, with a maximum intensity of VI-VII at Orihuela del Tremedal in the year 1848. Magnitudes usually range from 1.5 to 3.5, with maximum values of 4.4 in the Teruel Graben and 3.8 in the Albarracín massif (data from seismic database of Instituto Geográfico Nacional, IGN: https://www.ign.es/web/ign/portal/sis-catalogo-terremotos). Focal depths typically lie within the range of 5 to 15 km, which represents the brittle crust above the basal detachment identified by Roca and Guimerà (1992). Most of the available focal mechanisms correspond to normal faults and are consistent with the regional active stress field (Herraiz et al., 2000).

3. Materials and methods

3.1. Acquisition of structural data

Map-scale faults and fractures developed within the relay zone between the Concud and Sierra Palomera faults, with emphasis on those that show evidence of recent (Plio-Quaternay) activity, have been mapped with the help of aerial photographs (1:18,000 and 1:30,000 scales), satellite imagery (PNOA orthoimages, Instituto Geográfico Nacional, IGN; Google Earth) and Digital Elevation Models (5-m-resolution DEM from IGN) and field survey. Official maps published by the

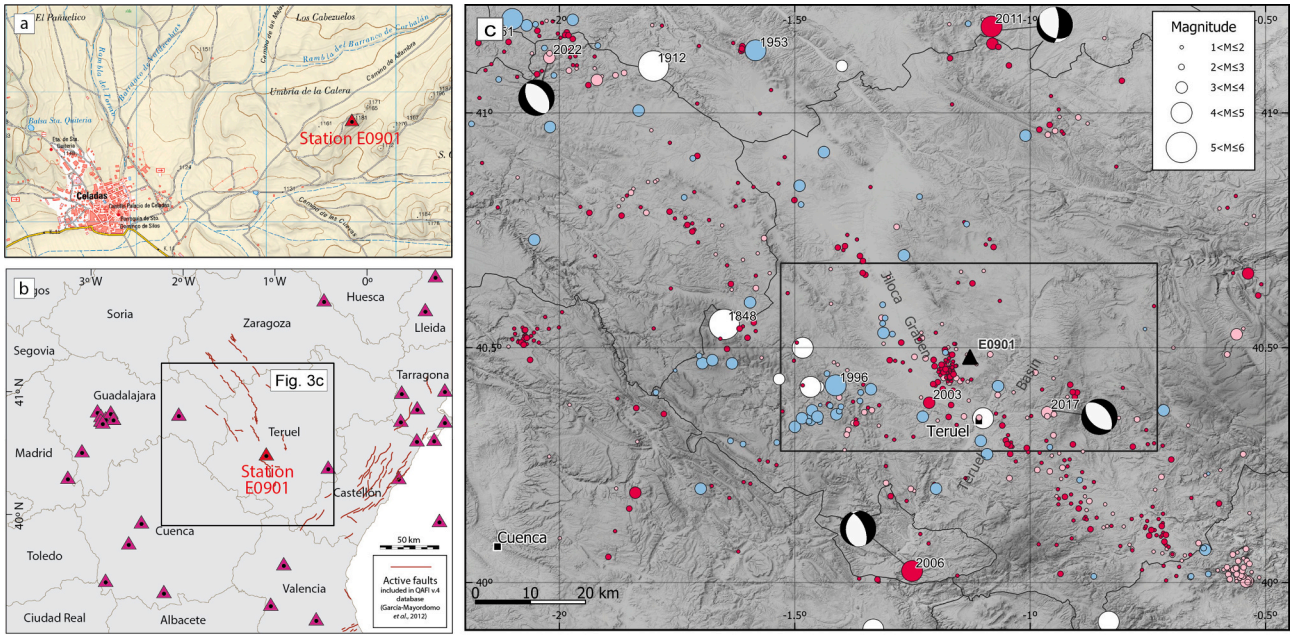

Fig. 3. (a) Location of seismic station E0901, east of Celadas, Teruel province (coordinates: 40° 28′ 50" N, 1° 07′ 41"W). Base map from the IGN National Topographic Map 1:25000 (MTN25). (b) Station E0901 within the seismic network of the central-eastern Iberian Peninsula. Red lines: Quaternary active faults included in the QAFI database, Quaternary Active Faults of Iberia, IGME, García-Mayordomo et al., 2012). See also Fig. 2b for location of Station E0901 within the geological framework. (c) Seismicity of the studied area. White dots: main historical earthquakes (1431–1923) with estimated magnitude Mw ≥ 3 (using relationships from Cabañas et al., 2015). Coloured dots: instrumental earthquakes from the IGN catalogue (https://doi.org/10.7419/162.03.2022); blue: earthquakes between 1923 and 2000; red: between 01/01/2000 and 13/07/2017; light pink: between 13/07/2017 and 30/05/2022. Black rectangle: area corresponding to the spatio-temporal and relocation analysis of the seismicity. Black triangle: E0901 Celadas seismic station. Focal mechanisms from IGN seismic database. Base map from the IGN CC-BY 4.0, ign.es. (For interpretation of the references to colour in this figure legend, the reader is referred to the web version of this article.)

Spanish Geological Survey (IGME) at 1:50.000 scale (Godoy et al., 1983a, 1983b; Hernández et al., 1983; Olivé et al., 1983; Ramírez et al., 1983) have been used as a start point. Field survey has also been carried out within specific sectors, in order to improve certain map details.

Outcrop observations have been made, at ten selected sites within Neogene and Quaternary materials, for characterizing the orientation and kinematics of mesoscale fractures and faults. Rose diagrams depicting their strike distributions have been elaborated using Stereonet software (Allmendinger et al., 2013; Cardozo and Allmendinger, 2013). Many of such minor fractures are nearly vertical and do not show any evidence of slip, so they have been interpreted as extension fractures (Mode I; Irwin, 1957) propagated orthogonal to the local σ_3 stress trajectories.

3.2. Seismic database (Spanish National Seismic Network)

The Spanish National Seismic Network of the Instituto Geográfico Nacional (IGN) is the organization responsible for seismic monitoring in Spain and neighbouring areas. In the first half of the 20th century, it started to perform this task by compiling the information of its geophysical observatories and the ones belonging to other institutions. In 1985, the Spanish Seismic Network was created, with eight seismic stations connected to the IGN central office. Since then, the number of stations has been increasing progressively. A qualitative leap was taken in 1999, when digital broadband seismometers were incorporated and the network started to conform to its current configuration. Since 1997, hypocentral locations are performed by LocSAT (Bratt and Naggy, 1991), although its implementation slightly changed in 2016, when SeisComP3 (GFZ, German Research Centre for Geosciences, and GEMPA GmbH, 2008) was adopted as earthquake monitoring system. The velocity model used for location is a 1D plane-parallel homogeneous layered model of continental-crust with a flat Moho at 31 km depth for the Iberian Peninsula (Mezcua and Martínez Solares, 1983) overlying the IASP-91 earth model (Kennett and Engdahl, 1991). The seismic catalogue and bulletins are made using all the available information from the IGN network and the networks of other institutions. The information from other networks has been gathered in the format of seismic arrival parametric data before 2016, and as continuous waveforms since this year. Currently, more than 150 seismic stations in the Iberian Peninsula are used to create the Spanish seismic catalogue. The station density of this whole virtual network is not homogeneous, since it is higher in the areas with higher seismic hazard (i.e., south and southeast of the Iberian Peninsula and Pyrenees). This allows detecting lower magnitude earthquakes with lower location uncertainties in these areas. By introducing LocSAT, in the second half of 1997, location uncertainty in the seismic bulletins is defined by a 90 % epicentral confidence ellipse (with a semi-major and a semi-minor axis; sMajAx and sMinAx) and a 90 % depth confidence interval (sDepth).

3.3. The new seismometer of Celadas

The anomalous increase in seismic activity recorded since 2014 in the area NW of Teruel, together with its seismotectonic interest, led the IGN to install a seismic station there (E0901). This new station was provisionally installed on 13/07/2017 in a site 2 km far from Celadas village (Teruel; Fig. 3a), with coordinates: 40° 28′ 50" N, 1° 07′ 41"W. The station lied on the floor of a small hermitage built in solid rough ashlar stone. This is a sparsely inhabited area (around 400 people) located less than 10 km north of the Concud fault trace, and more than 60 km to the closest seismic station (Fig. 3b). The station was equipped with a Guralp CMG-6TD three-component digital broadband (0.03 Hz – 100 Hz) seismometer and replaced on 18/10/2018 by a Nanometrics Trillium Compact three-component broadband (0.0083–100 Hz) sensor and a Nanometrics Centaur digital recorder. The availability of data from 13/07/2017 to 22/06/2022 is 93.3 %.

3.4. Spatio-temporal analysis and magnitude of completeness

A general characterization of the spatial-temporal evolution of the seismicity has been performed. The region considered for this analysis is constrained between 40.28°N and 40.68°N in latitude, and between −1.53°W and − 0.73°W in longitude (rectangle within Fig. 3c), and to a temporal period ranging from the 1st of January 2000 to the 25th of May 2022. The total number of events used in this analysis is 171. Calculations have been performed by using the Zmap7 software package (Wiemer, 2001). For reasons of homogeneity, in this analysis it has been assumed that $M = M_w$.

On the one hand, the frequency–magnitude earthquake distribution of this catalogue was analysed by means of the Gutenberg–Richter (GR) relationship.

$$log\ N = a – b\ m$$

being N = number of events with magnitude ≥ m (Gutenberg and Richter, 1944). In this relationship, the *a-value* characterizes the seismicity in the region, with a *high a-value* corresponding to high seismicity. The *b-value* is the slope of the GR relationship and represents the relative number of earthquakes of different magnitudes in the given area (the larger the b-value, the higher the number of smaller events). The *b-value* varies both temporally and spatially (regionally and with depth). To estimate these GR parameters (a-value, b-value) the maximum-likelihood approach (Aki, 1965) has been used (Fig. 4).

A *b-value* of 0.73 ± 0.04 has been obtained, being consistent with the typical values of this parameter (usually in the range of 0.6–1.1 for natural seismicity). Although the GR law seems to fit properly between M 1.4 and 2.25, it can be highlighted that the line does not fit well the larger magnitudes. This deviation of the largest earthquakes in the study area from a linear frequency-magnitude may reflect that the sampling used is too small and insufficient to estimate the b-value in a reasonable way for the largest events. This effect can be seen in cases where the number of large earthquakes in the analysed area is small (Stein and Wysession, 2003).

For this kind of seismicity-based studies, assessment of the magnitude of completeness of the seismic record (Mc) is essential. Mc can be defined as the lowest magnitude at which 100 % of the events in a space-time volume are detected (Rydelek and y Sacks, 1989). In this study, the Mc value has been estimated with the maximum curvature method (Wiemer and Wyss, 2000), a fast and simple way to calculate Mc that is implemented in the Zmap7 software (Wiemer, 2001). According to this method, Mc corresponds to the point of maximum curvature by computing the maximum value of the first derivative of the frequency-magnitude curve (Mignan and Woessner, 2012). This means that Mc matches the magnitude with the highest frequency of events in the non-cumulative Frequency Magnitude Distribution (FMD). The seismic catalogue is considered to be complete when it considers the events with M ≥ Mc. This means that a fraction of events with M < Mc can have occurred but might be missed by the seismic network. For this reason, earthquakes with M below Mc, estimated at 1.4 for this study (Fig. 4), have not been considered. The resulting catalogue contains 132 events of M ≥ Mc.

Once the seismic catalogue has been filtered and considered as complete, the temporal evolution of the seismicity has been analysed to detect possible changes or trends of seismicity patterns. For this, the number of events and their magnitudes by date, as well as the cumulative number of events versus time are considered. Seismic activity is a process of energy accumulation and release, and so the cumulative seismic moment release by earthquakes with M ≥ Mc has also been computed. The area used for building the cumulative rate and moment release graphics is the same as for the Gutenberg-Richter model.

3.5. Improvement in earthquake detectability due to the new E0901 station

In order to analyse the improvement that the Celadas station entails, two periods of data from the seismic catalogue have been compared: a first one that ranges from 01/01/2000 to 13/07/2017, and a second one from 13/07/2017 to 30/05/2022 (prior and subsequent, respectively, to the new E0901 seismic station). The area that has been firstly considered for this purpose is broader than the Iberian Chain (latitude between 39°N and 42°N and longitude between 4°W and 1°E; Fig. 3b). Within it,

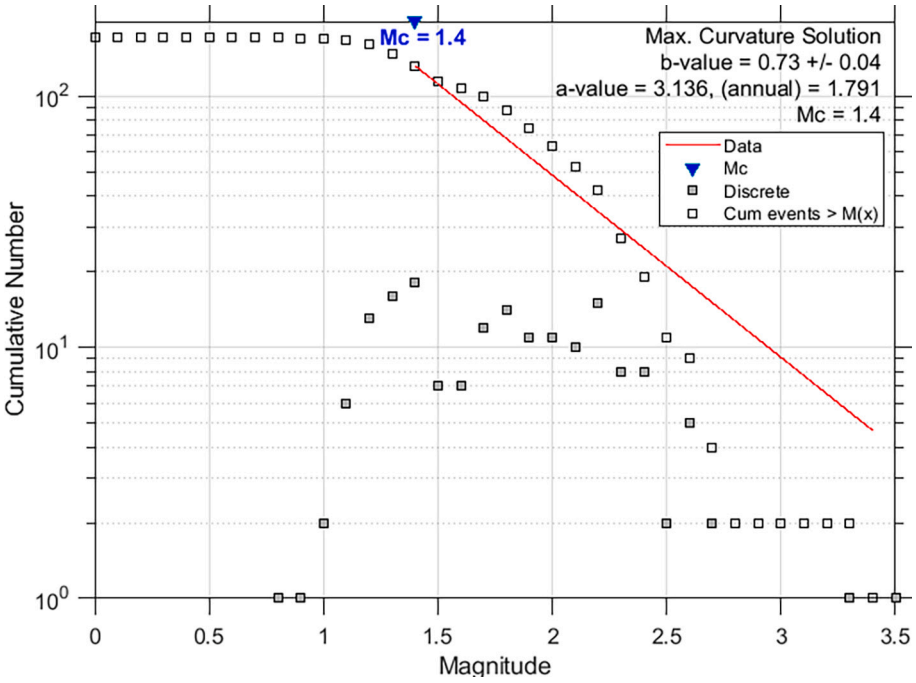

Fig. 4. Magnitude-frequency relationship of seismic events recorded in the study area (40.28°N to 40.68°N; −0.73°W to −1.53°W) fitting the Gutenberg-Richter law. Data source: National Geographic Institute (IGN), Spanish seismic catalogue: https://doi.org/10.7419/162.03.2022. Grey squares: distribution of non-cumulative number of events; white squares: cumulative number of events. Mc = 1.4 is the inferred magnitude of completeness (see main text for further explanation).

the catalogue includes a total of 3324 and 1303 events in the first and the second period, respectively, which means 190 and 267 events per year. For this region, the magnitude of completeness (Mc) is around 1.6 for both periods.

Spatial locations of these 2000–2022 events are the original ones from the Spanish seismic catalogue. The average epicentral uncertainties sH (from sMajAx and sMinAx values) and sDepth of the events with a Mw $\geq$ 2.0 have been computed for both periods, their spatial distributions being depicted in Fig. 5. When a more constrained area around E0901 station is considered (latitude between 40.28°N and 40.68°N and longitude between −1.53°W and − 0.73°W; rectangle within Fig. 3c), we find a total of 125 and 46 events for the whole range of magnitudes in the first and second periods, which means around 7 and 9 events per year, respectively.

In both cases (region depicted in Fig. 5, and area constrained around E0901 station) the seismic network has been capable of locating more events per year since the installation of the E0901 station. Such increase in the number of events in the catalogue should respond to a higher earthquake detectability. Moreover, epicentres of these events are now better constrained because their location uncertainties have clearly decreased in the second period with respect to the first one in the whole area and, more specifically, in the surroundings of the E0901 station (from 2.1 to 4 km, in the first period, Fig. 5a, to $\leq$3 km, in the second one, Fig. 5b). However, there is no visible improvement in their location in depth (Fig. 5c,d), probably because of the different implementation of LocSAT before and after 2016.

3.6. Absolute relocation using a nonlinear probabilistic method

In order to avoid any possible heterogeneity derived from this different implementation of LocSAT, and to improve the hypocentral solutions, an absolute relocation of the whole period (01/01/2000 to 30/05/2022) has been carried out using the nonlinear probabilistic location method NonLinLoc, NLL (Lomax et al., 2000). The NLL method allows to estimate the "optimal" (the maximum likelihood) hypocentres and the probability density function of each event location, providing a complete information on the location uncertainties using an inversion approach (Tarantola and Valette, 1982).

Moreover, with the aim of testing the possible dependency of the resulting location with the velocity model used, this relocation has been done using two different 1D velocity models (see Fig. 6a): (i) the laterally homogeneous 1D continental crust velocity model for Iberia used by IGN (Mezcua and Martínez Solares, 1983); (ii) a local 1D velocity-depth distribution for the Iberian Chain extracted from the study by Diaz and Gallart (2009) on the crustal structure beneath the Iberian Peninsula, derived from deep seismic profiles. In both cases we assumed a constant vp/vs ratio of 1.75. The main differences between these two models are as follows: the second one is slower, and its crust extends 8 km deeper than the first one.

We have relocated a total of 134 M $\geq$ 1.4 events recorded in the constrained area (same region specified in Section 3.4, see Fig. 3c) for the whole study period with more than 10 picked phases each, ensuring well-constrained solutions. These picks are P and S wave first arrivals extracted from the IGN catalogue and recorded at 264 stations located

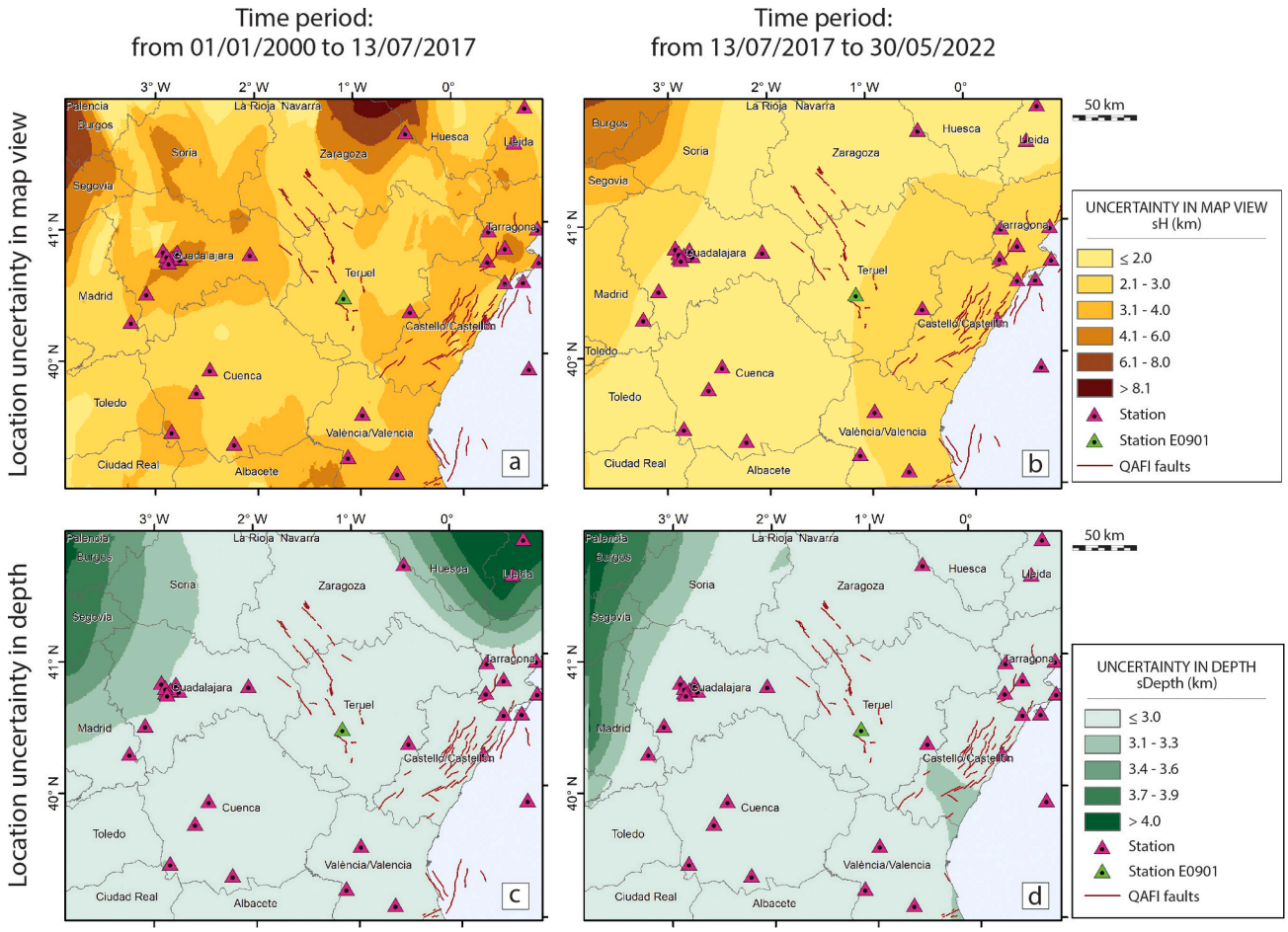

Fig. 5. (a, b) Spatial distribution of location uncertainties in map view (sH) of epicentres of events with Mw $\geq$ 2.0 computed for the two studied periods. (c, d) Spatial distribution of location uncertainties in depth (sDepth) of events with Mw $\geq$ 2.0 computed for the two studied periods. Main active faults (those included in the QAFI database; García-Mayordomo et al., 2012), seismic network and, specifically, location of station E0901, are shown.

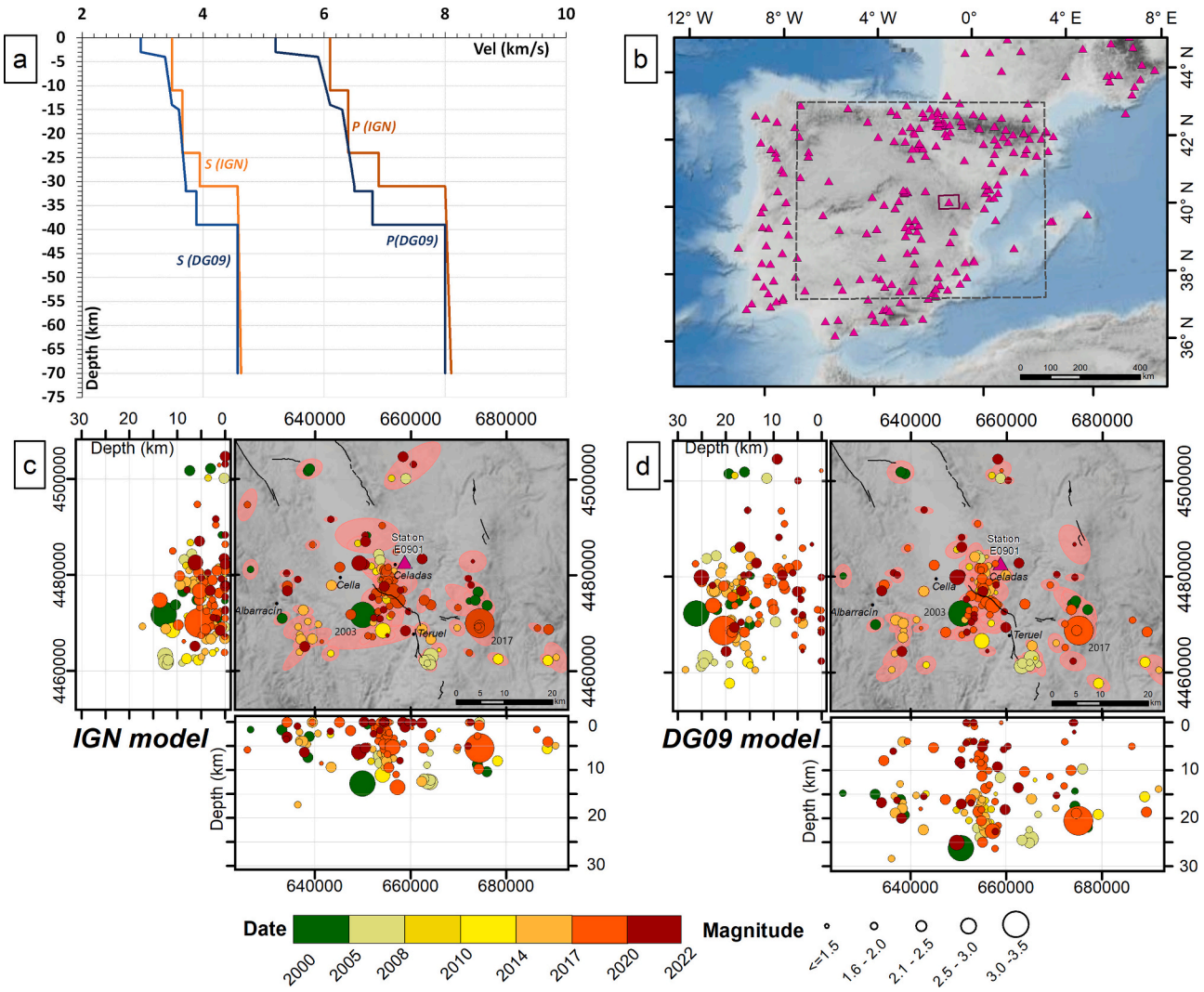

Fig. 6. (a) P-wave and S-wave profiles for the 1D velocity models used for NLL relocation: IGN model (orange lines) and DG09 model (blue lines); (b) Seismic stations within the velocity model grid (large rectangle) used for the absolute relocation with NLL; (c,d) NLL maximum likelihood relocated hypocentres in the Teruel area (small rectangle in b), based on the IGN model and DG09 model, respectively (map view and projections onto vertical north-south and east-west planes). Four earthquakes have depths deeper than 30 km when the DG09 model is used. Hypocentres are represented by dots, coloured according to their origin date, and sized according to the magnitude. Error ellipses for a 90 % confidence level are also plotted. Black lines represent main Quaternary active faults (those included in QAFI v.4 database, Quaternary Active Faults of Iberia, García-Mayordomo et al., 2012). (For interpretation of the references to colour in this figure legend, the reader is referred to the web version of this article.)

inside the model grid (Fig. 6b). The epicentral distances of these seismic stations range between 2 and 950 km, and the azimuthal gap between 30° and 290°. Observations with large time residuals (>2.0 s) have been removed and station delays have been included as station corrections in the relocation process, in order to reduce the influence of nonmodeled propagation effects due to local surface geology and lateral heterogeneities.

In order to analyse the spatial distribution of the seismicity, the location of hypocentres has been considered, together with their uncertainty ellipses with a 90 % confidence level (represented by the semi major and minor axes, sMajAx, sMinAx, of the epicentral uncertainty ellipses, and the depth uncertainty, sDepth). Using Geographic Information Systems (GIS), these hypocentral locations and their associated uncertainties have been translated into both a map based on a Digital elevation Model (DEM) of the study area, and two vertical projections (N-S and *E*-W) that show their depths and associated uncertainties (see Fig. 6b,c). The study area considered for this spatial analysis is more constrained in order to only encompass the southern sector of the Jiloca graben, where the relay zone between the Concud and Sierra Palomera is located.

4. Structural results: Overall structure and fracture patterns at the relay zone between the Concud and Sierra Palomera faults

A number of recent fault segments have been identified and mapped at the relay zone separating the Concud and Sierra Palomera faults, on the basis of one or more of the following criteria: (i) they cut and offset one of the Pliocene planation surfaces that extend through the region (Fundamental Erosion Surface; sublevels FES2 and FES3), dated between 3.8 and 3.5 Ma (Simón-Porcar et al., 2019; Ezquerro et al., 2020); (ii) they produce abrupt and straight map contacts between Quaternary and pre-Quaternary materials, which have been inspected through image analysis and field survey; (iii) they have associated morphological scarps.

The traces of such recent fault segments (apart from the master faults themselves) typically have ~4 km in length, and trend NW-SE to NNW-SSE (Fig. 7a,b). From north to south, we can highlight: (i) La Peñuela fault; (ii) Las Vallejadas fault; (ii) Montero monocline, probably

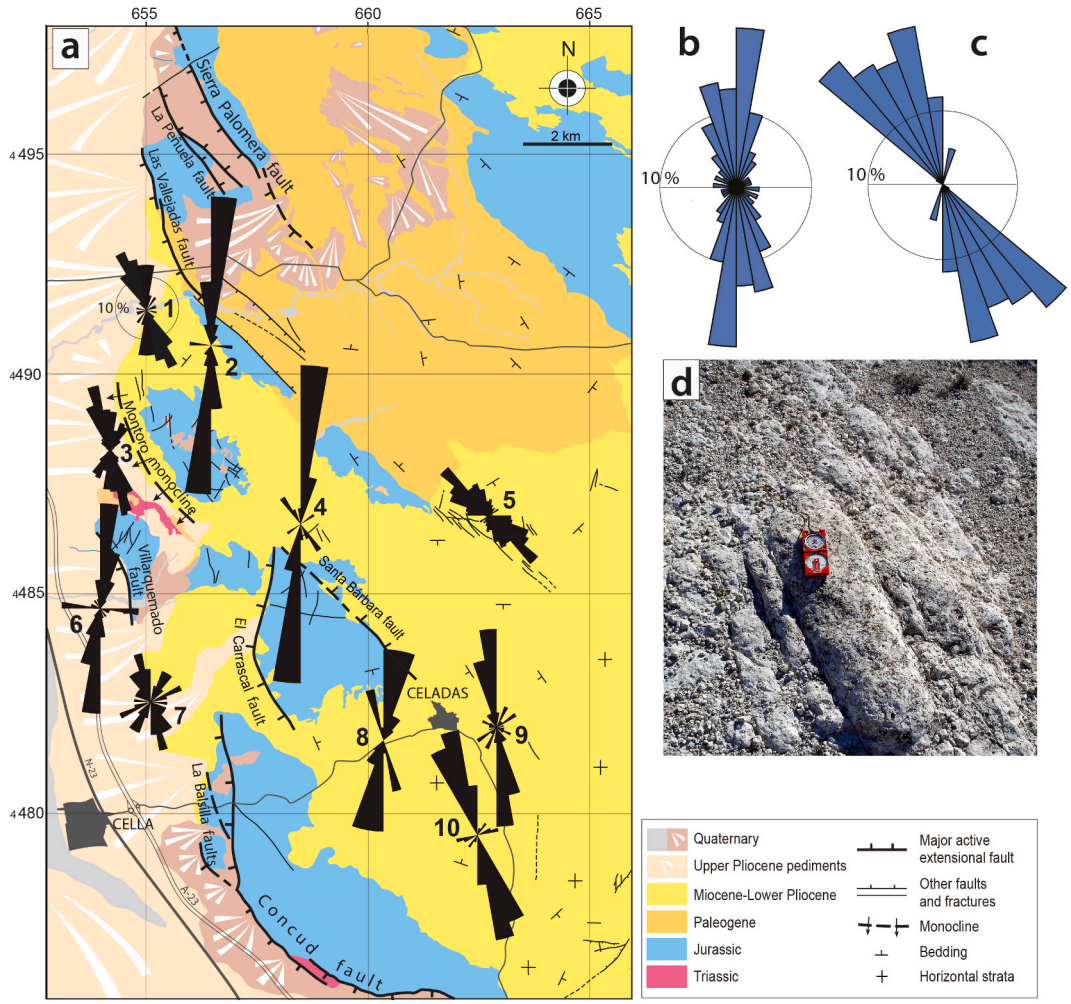

Fig. 7. (a) Structural map of the relay zone between Sierra Palomera and Concud faults (see location in Fig. 2b), with rose diagrams showing the strike distributions of mesostructural fractures (joints and small faults) collected in ten sites within Neogene and Quaternary units. Mesostructural data sources: sites 1–3 and 6–10 from Peiro et al. (2020); sites 4–5 from Ezquerro (2017). (b) Synthetic rose diagram of strike distribution of mesoscale fractures from sites 1–10. (c) Idem for map-scale recent faults mapped in a (weighted according to their lengths). (d) Example of nearly vertical joints cutting Neogene limestones in site 10 (compass, 20-cm long, oriented to the North). (For interpretation of the references to colour in this figure legend, the reader is referred to the web version of this article.)

developed above a blind fault; (iii) Villarquemado fault; (iv) Santa Bárbara fault; (v) El Carrascal fault, made of two oblique segments that trend NNE-SSW and NNW-SSE, respectively; (vi) La Balsilla fault segments, N-S to NNW-SSE striking, and branching out from the tip of the main Concud fault. Except for La Peñuela and Santa Bárbara faults, the rest are synthetic with the Concud and Sierra Palomera faults.

La Balsilla fault segments represent a prolongation of the Concud fault trace previously mapped (Hernández et al., 1983; Lafuente, 2011; Lafuente et al., 2011a, 2014). In this way, the length of the Concud fault, which had been measured at 14.2 km (Lafuente et al., 2014), could attain ~17 km indeed. The Villarquemado, Santa Bárbara and El Carrascal faults had not been mapped in the above-mentioned works, neither the Montoro monocline, and they were only partially incorporated by Peiro et al. (2020). Therefore, the map of Fig. 7a provides a new structural setting, in which the relay zone reveals itself to be more complex than previously thought. Overall, the fracture setting suggests an incipient tendency to fault linkage of the Concud and Sierra Palomera master faults by means of multiple along-strike fractures, i.e., fitting the model proposed by Peiro et al. (2020).

Although none of these faults show outcropping rupture surfaces with slickenlines, we will assume for them a nearly pure dip-slip normal movement based on (i) the regional persistence of this type of fault kinematics (e.g., Simón, 1983, 1989; Simón et al., 2012, 2022; Lafuente et al., 2014; Liesa et al., 2019; Peiro et al., 2022), and (ii) the focal mechanisms available in the surrounding area (see Fig. 3c), as we will explain in the Section 6.

Concerning fractures observed at mesoscopic scale (e.g., Fig. 7d), we here summarize the data acquired by Peiro et al. (2020) in eight sites, which include orientations of a total of 371 nearly vertical joints cutting Upper Miocene conglomerates (site 2), Mio-Pliocene limestones (sites 6, 7, 8, 9 and 10), Upper Pliocene lutites and marls (site 3), and Plio-Quaternary alluvial clastics that unconformably overlie the latter (site 1). We have also compiled the results from two small areas for which Ezquerro (2017) provided detailed mapping of 224 hectometre-scale Neogene fractures (sites 4 and 5). In Fig. 7a, we reproduce the original rose diagrams depicted in those articles; the nearly vertical attitude of all fractures makes the use of stereograms unnecessary. The synthetic rose diagram depicted in Fig. 7b shows that N-S and NNW-SSE striking fracture sets clearly prevail on an outcrop scale.

The directions of map-scale and outcrop-scale fractures are partially parallel to each other. If we compare the synthetic rose diagrams of Fig. 7b and c, we can distinguish three conspicuous sets: (i) a NNW-SSE set that appears at both scales; (ii) a N-S to NNE-SSW set prevailing for mesofractures; (iii) a NW-SE set prevailing at map scale, although it is also locally dominating at outcrop scale (site 5). Frequently, secondary cross-joints accompany and abut at right angles the N-S prevailing joints

(sites 1, 2, 6, 7 and 10).

5. Seismological results

Relocated events with the IGN velocity model and the Diaz and Gallart, 2009 model (DG09) are shown in Fig. 6c and d, respectively. Epicentral distribution is very similar in both cases, with a mainly N-S alignment of epicentres and most of the events located within the relay zone between the Concud and Sierra Palomera faults. A comparison of both solutions indicates that there is not a significant displacement of epicentres and that such displacement does not follow any clear spatial pattern (see Fig. SM-1 included in Supplementary Material). On the contrary, a spatial randomness on the epicentral displacements between both solutions is observed. In addition, most of these shifts lie within the corresponding error ellipse. These results give us an idea of the robustness of the epicentral solution, as we do not observe any systematic bias when using two different earth models that could be applied to our study area.

Depth distribution of hypocentres (left and bottom panels in Fig. 6c, d) shows that, in the case of the IGN velocity model, seismicity is concentrated in the upper crust (h < 20 km) with most of the events located between 1 and 15 km. Nevertheless, with the DG09 model, the

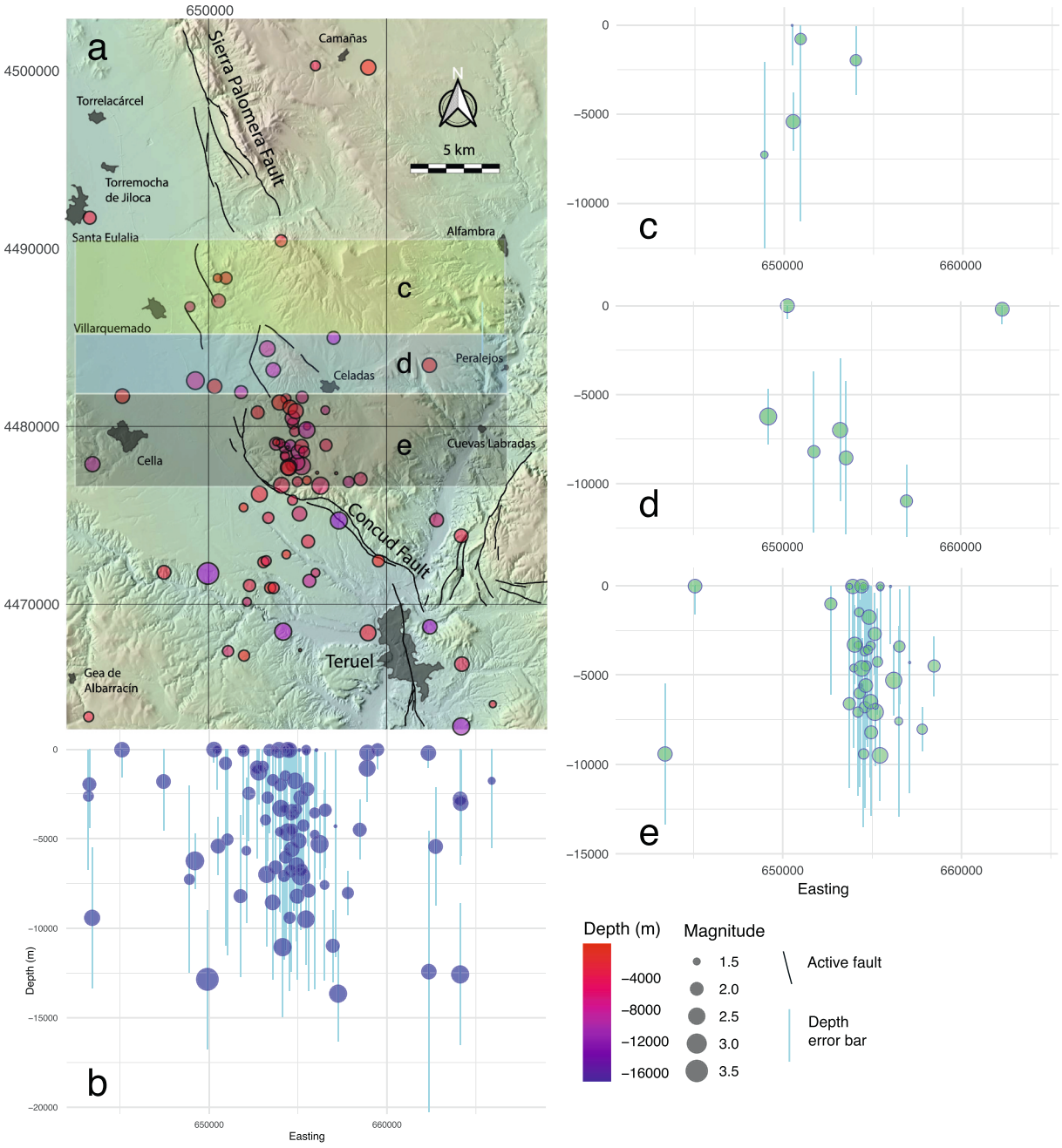

Fig. 8. Close view to the relationship between relocated hypocentres in the period 2000–2022 (IGN model) and recent faults (see location in Fig. 2b). (a) Map view (see location in Fig. 2b). Epicentral symbols are colour coded with depth, and sized according to their magnitude. The active faults mapped are those included in the QAFI database (García-Mayordomo et al., 2012), together with others described in detail in more recent publications (Simón et al., 2016, 2017, 2019; Ezquerro et al., 2020; Peiro et al., 2022) and those newly mapped in the present work. (b) Synthetic projection of all hypocentres onto a vertical *E*-W plane. Dots and segments indicate the depths and their uncertainties. (c), (d) and (e) Partial projections, onto vertical E-W planes, of hypocentres located within the corresponding strips on the map.

hypocentres oscillate in a wider depth range, most of them extending down up to 30 km (moreover, four foci are located between 30 and 50 km, not represented in the figure). This difference can be due to the slower velocities of the DG09 model, which could be accommodated either by a larger hypocentral depth or an earlier origin time.

It is important to highlight that, regardless the velocity model used, a clear near-vertical alignment in depth can be observed in the cluster of events situated in the relay zone.

Therefore, regarding the current results, the relocation with the 1D IGN model is considered as the most reliable solution because focal depths are more consistent with the thickness of the brittle crust above the basal detachment (Roca and Guimerà, 1992), and better fit geological parameters. Moreover, the use of a regional model (1D IGN) instead a local model (DG09) seems to be more suitable due to: (i) the wide model grid considered for the selection of the seismic stations, and (ii) the resulting location uncertainties (in average terms), which are slightly smaller than those from the DG09 model. It must be noticed that, when comparing both velocity models, the uncertainty in depth is still high regardless the model used for the relocation, due to the poor station coverage with only a few stations close to the epicentres.

In general terms, the relocation using the absolute nonlinear probabilistic location method has substantially improved the IGN hypocentral locations, providing depth solutions for over 50 events previously characterized with fixed depth in the original IGN catalogue. Furthermore, no hypocentral depths associated with the different layers of the model are observed as in the original IGN catalogue. Finally, location uncertainties have decreased after installing the Celadas station, with significant improvement in the average values of both sH (from 3.4 to 2.4 km) and sDepth (from 4.4 to 2.7 km), compared with to those obtained with the rutinary location of the IGN (see Fig. 5).

In order to associate the seismicity with the main active faults of the area, a smaller spatial window is considered (40.31°N, 40.66°N; −1.01°W, −1.32°W) (Fig. 8a). Within the period 2000–2022, 87 events with $1.4 < Mw \leq 3.5$ have occurred in the selected area. The most conspicuous seismic cluster appears within the relay zone between the Concud and Sierra Palomera faults, at the footwall block of the Concud fault. The epicentres delineate a nearly N-S trending band, which is not far from the northern segment of the Concud fault; it is about 2–3 km wide and extends for about 10 km northwards.

The hypocentre cluster is also clearly visible in the synthetic projection onto a W-E vertical plane (Fig. 8b). It is therefore compatible with a nearly vertical fault or, more probably, fault zone. In order to visualize the distribution of hypocentres within the relay zone and explore their possible spatial variation, three separate projections have been made, each one gathering the seisms located within a map strip. Strips have been delineated across distinct faults: Montoro monocline and Villarquemado fault (Fig. 8c), El Carrascal and Santa Bárbra faults (Fig. 8d), and northern sector of the Concud fault (Fig. 8e). Clustering is more conspicuous close to the Concud fault trace, at its footwall block (Fig. 8e), while it vanishes northwards (Fig. 8c,d). In any case, individual seisms can not be associated with the faults mapped. Concerning their depth distribution, it should be highlighted that the hypocentres are quite uniformly distributed between 0 and 14 km, which is consistent with the thickness of the brittle crust above the regional detachment level of the main fault systems (11–17 km, according to Roca and Guimerà, 1992, and Ezquerro et al., 2020). For a better, 3D visualization of the spatial distribution of hypocentres, a html file is available as Supplementary Material (SM-2).

Regarding the temporal distribution of the seismic activity within the study area, it seems to have had moderate increases in two time periods (Fig. 9a): 2005–2008 (segment 2 in Fig. 9b) and 2014–2022 (segments 4 and 5 in Fig. 9b). Within the latter, two different periods can be distinguished: one up to 2018, when the highest seismic activity occurred within the study area, with a special increase in year 2016 (Fig. 9a; segment 4 in Fig. 9b), and another period until now, corresponding with a still increasing but less noticeable activity (segment 5 in

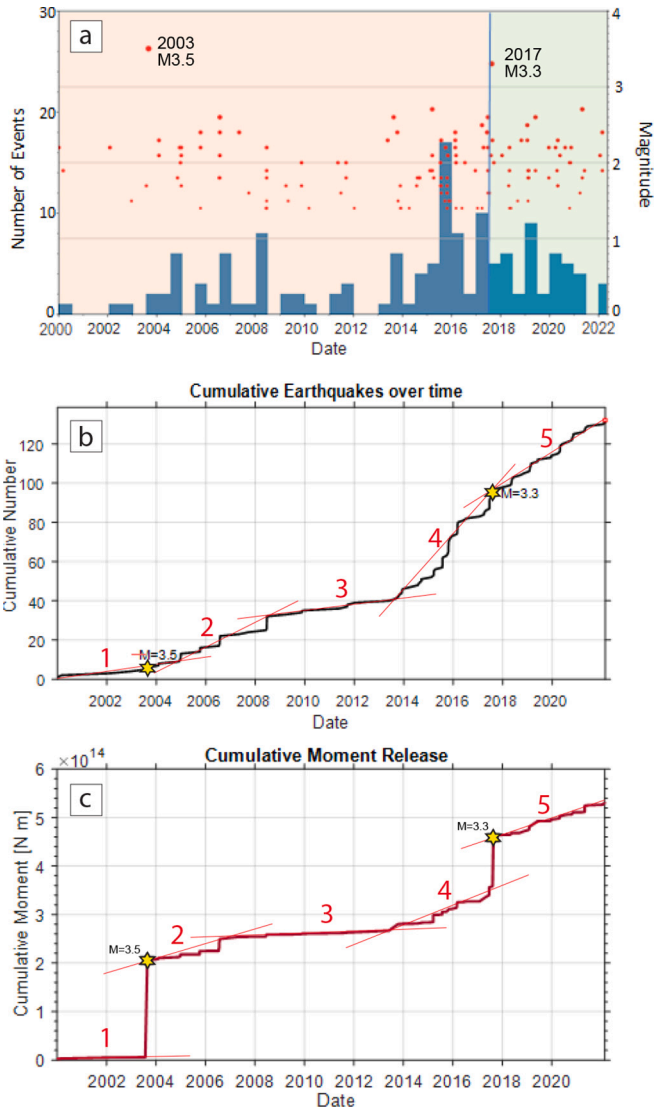

Fig. 9. (a) Histogram of temporal distribution of events within the study area for the 2000–2022 period. Blue bars: number of events; red dots: magnitude. Earthquakes recorded before and after the installation of station E0901 in 2017 are shown on orange and green background, respectively. (b) Cumulative number of events with M ≥ Mc. Segments 1–5 correspond to different graphic slopes and, therefore, changes in seismic activity. (c) Cumulative seismic moment release over time for events with M ≥ Mc. Segments 1–5 correspond to different graphic slopes. Yellow stars: events of M > 3.0. (For interpretation of the references to colour in this figure legend, the reader is referred to the web version of this article.)

Fig. 9b). These two main periods of higher number of events correlate well with two periods of higher seismic energy liberation (segments 2, 4 and 5 in Fig. 9c). In this context, two earthquakes are remarkable: one occurred 10 km to the WNW of Teruel city in 2003 with M3.5 (Figs. 3c, 6c,d and 9), and another one occurred 12 km to the E of Teruel city in 2017 with M3.3 (Figs. 3c, 6c,d and 9).

6. Interpretation and discussion

The gentle, wide relay ramp between the Concud and Sierra Palomera faults is cut by a number of faults and fractures propagated, since Late Pliocene-Pleistocene times, nearly parallel or at small angles to the master faults. Such along-strike distributed fracture pattern closely fits the model of fault coalescence proposed by Peiro et al. (2020) (Fig. 1). This model essentially involves externally controlled fracturing,

responding to the remote stress field and, to a lesser extent, to the structural inheritance, with negligible contribution of the internal relay kinematics.

Considering the consolidated model of the recent regional stress field (Simón, 1982, 1983, 1989; Arlegui et al., 2005; Liesa et al., 2019; Simón et al., 2022; see Section 2), the NNW-SSE striking fracture sets (recognized at both map and outcrop scale) undeniably respond to the remote stress field, since they are orthogonal to the dominant σ_3 trajectories. In addition, the prevailing N-S to NN*E*-SSW mesofracture set should also be attributed to the regional extension, whose σ_3 trajectories occasionally trend E-W to ESE-WSW (Liesa et al., 2019; Simón et al., 2022). Finally, propagation of the NW-SE striking fault segments (as well as locally observed mesofractures parallel to them) was probably controlled by faults inherited from the Paleogene compressional stage, then reactivated as normal faults under the recent extensional stress field.

The persistence of such stress field and faulting patterns at the present time is supported by focal mechanisms. Owing to the low magnitude of seisms recorded during the recent instrumental period, only four focal mechanisms are available from the IGN seismic database (https://doi.org/10.7419/162.03.2022) for the surrounding region (central Iberian Chain, see Fig. 3c). However, they constitute robust solutions and show a remarkable homogeneity. The nodal planes strike NNW-SSE to N-S, the fault plane being probably represented by that with steeper dip (N-S striking in the case of the 2011 seism, north of Fig. 3c; NNW-SSE in the other cases). All focal solutions correspond to nearly pure dip-slip normal faults, which is consistent with the kinematics inferred for surface faults throughout the region (e.g., Simón, 1983, 1989; Simón et al., 2012, 2022; Lafuente et al., 2014; Liesa et al., 2019; Peiro et al., 2022). The ensemble of focal mechanisms is fully compatible with the regional extensional stress field (σ_1 vertical, σ_3 trending WSW-ENE), evidenced for both recent geological times (Simón, 1983, 1989; Arlegui et al., 2005; Liesa et al., 2019; Simón et al., 2022) and the present day (Herraiz et al., 2000).

The imprint of the inherited fault directions can be particularly noteworthy within a radial or multidirectional extensional stress field (σ_1 vertical, $\sigma_2 \approx \sigma_3$), as that inferred at the central-eastern Iberian Chain (Simón, 1982, 1983, 1989; Arlegui et al., 2005; Liesa et al., 2019). Within such stress regime, the differential stress in the horizontal plane is small, and hence freedom for any pre-existent fault to be reactivated is high. Nevertheless, it is noteworthy that, even under such stress regime, the influence of the remote σ_3 direction has prevailed. On the contrary, NE-SW striking faults or fractures, which could be expected in the case of fracturing induced by relay kinematics, are virtually absent at all scales (see Fig. 6a).

The same evolutionary pattern is evidenced at the neighbouring narrow (1.3 km wide) relay zone between the Concud and Teruel faults (Peiro et al., 2017, 2020). All the more reason to expect in a wide relay zone as that between the Concud and Sierra Palomera faults (ca. 8 km, measured orthogonal to the fault traces; ca. 11 km in distance between fault tips), where the local kinematic-dynamic conditions induced by the master faults are surely negligible when compared with the regional stress field.

Viewed as a whole, the Concud fault shows three distinctly oriented segments: a NW-SE central segment and two NNW-SSE end ones (Fig. 2b). The central segment resulted of negative inversion of a Paleogene thrust (structural inheritance; Lafuente, 2011; Lafuente et al., 2011a), while the other two would represent recent, southwards and northwards propagation controlled by the coeval stress field.

Such evolutionary tendency, in which the influence of the remote extension gradually substitutes the imprint of the structural inheritance as the faults propagate, was already highlighted and conceptualized by Anders and Schlische (1994). These authors provide examples from both ancient and recent extensional structures. In the early Mesozoic Newark basin (New Jersey and Pennsylvania, USA), intrabasinal splay faults propagate orthogonal to the coeval extension direction, therefore forming an angle with the master, ancient faults (Schlische, 1992). The same occurs in the Beaverhead fault (Idaho, USA), in this case evolving through Neogene to Quaternary times.

The present-day seismic activity of the Celadas area can be interpreted within this structural and tectonic setting. The epicentres located within the relay zone between the Concud and Sierra Palomera faults are visibly gathered in a N-S trending cluster (Fig. 8a). Although the hypocentral distribution does not allow the precise definition of the fracture geometry, its aspect in a projection on a vertical, W-E striking plane (Fig. 8b,e) suggests the occurrence, below the surface, of either a single fault or a fault zone with a nearly vertical attitude. Their location and orientation allow therefore assign them to the same fracture system that characterizes the relay zone at the surface, although they do not correspond to any of the individual faults mapped in Fig. 6a.

In summary, the analysed seismic cluster evidences how the evolutionary pattern proposed by Peiro et al. (2020) for the Concud-Sierra Palomera fault relay since Late Pliocene-Pleistocene times is currently operating. Moreover, as in the example reported by Bawden et al. (1999) near the Big Bend segment of the San Andreas fault, the instrumental seismicity suggests that subsurface fracture propagation is progressing beyond what the discontinuous mapped faults reveal.

Concerning the hypothetical temporal patterns of seismic activity, their relevance for the regional seismotectonic framework is doubtful. The moderate increases in the seismic activity in the 2005–2008 and 2014–2022 periods (Fig. 9), evoke the succession of alternating periods of fast and slow slip rate recorded at the Concud fault at the scale of 10^4 years (Simón et al., 2016). Obviously, the respective time scales are quite different, but it is suggestive to conceive fractal, self-similar behaviour of fault activity in time, which could reproduce the fractal character of the geometry of fracture systems through distinct spatial scales (Turcotte, 1986). Nevertheless, time scales of such fluctuations are too small in comparison with the duration of fault linkage processes developed in the region from Pliocene times. Therefore, it does not seem cautious to draw further conclusions on the possible implications of these temporal variations in seismicity on the proximal evolution of the relay zone between the Concud and Sierra Palomera faults.

7. Conclusions

(1) The relay zone between the Concud and Sierra Palomera faults is a complex relay ramp articulated by a number of shorter, NW-SE to NNW-SSE striking faults accompanied by NNW-SSE to NN*E*-SSW mesoscale fractures. The overall fracture pattern suggests an incipient tendency to fault linkage of both master faults, the displacement being transferred through a gentle relay ramp mostly cut by along-strike distributed faults and fractures. The latter are externally controlled, responding to the remote stress field (fracture traces orthogonal to the σ_3 trajectories) and, to a lesser extent, to the structural inheritance (fracture traces nearly parallel to Paleogene contractive faults).

(2) The episodes of increasing seismic activity in the study area during 2005–2008 and 2014–2022 can be considered as real. The quality of the instrumental seismic record north of the Concud fault has been significantly improved by a new seismic station installed near Celadas, but such increasing activity has not been spuriously induced by the improvement in earthquake detectability.

(3) The relocation process using the absolute nonlinear probabilistic location method shows an improvement over the IGN hypocentral location, providing better depth constraint than the IGN catalogue. In addition, it employs a more refined uncertainty estimation and homogenizes the results over the studied period with respect to the location program.

(4) The robustness of the 3D spatial distribution of the seismicity, with no systematic bias regardless the 1D velocity model used, has been proven. The solutions obtained with the 1D IGN regional model fit better the geological data and the thickness of the brittle

crust expected for this area than the ones obtained with a local model for the Iberian Chain.

(5) Regardless the velocity model used for relocation, a conspicuous cluster of epicentres occurs along a nearly N-S trending band located north of the Concud fault and SW of the Celadas seismic station. Focal depths range from 0 to 14 km. This 3D spatial distribution of seismic foci is interpreted as a consequence of activation of either a single extensional fault or a fault zone; in any case, they are N-S striking, nearly vertical, and deeply rooted in a crustal-scale discontinuity. In addition, it provides insight into the active seismogenic depth, and is in good agreement with independent (structural and geophysical) estimates of the brittle crust thickness in the region.

(6) It is very difficult to associate individual hypocentres to individual mapped faults. Nevertheless, the deep structure responsible for that seismic cluster should be genetically and functionally linked to the surficial N-S to NNW-SSE striking fault and fracture system observed at all scales. All of them are optimally oriented to the ENE-WSW to E-W trending σ_3 trajectories of the regional stress field, and they represent complementary expressions of the same fault propagation process at the Concud-Sierra Palomera relay zone. In this way, the present-day seismic activity evidences how the evolutionary model proposed by Peiro et al. (2020) for the coalescence tendency at the Concud-Sierra Palomera fault relay, i.e., along-strike fault propagation under the control of remote stress, is currently operating.

Supplementary data to this article can be found online at https://doi.org/10.1016/j.tecto.2024.230541.

CRediT authorship contribution statement

Alba Peiro: Writing – review & editing, Writing – original draft, Validation, Methodology, Investigation, Data curation. **Lucía Lozano:** Writing – review & editing, Writing – original draft, Validation, Supervision, Methodology, Investigation, Formal analysis, Data curation, Conceptualization. **Luis E. Arlegui:** Writing – review & editing, Writing – original draft, Validation, Software, Methodology, Investigation, Formal analysis, Data curation. **Juan V. Cantavella:** Writing – review & editing, Writing – original draft, Validation, Supervision, Methodology, Investigation, Formal analysis, Data curation, Conceptualization. **Sandra Ruiz-Barajas:** Writing – review & editing, Writing – original draft, Validation, Methodology, Investigation, Formal analysis, Data curation. **José L. Simón:** Writing – review & editing, Writing – original draft, Supervision, Project administration, Methodology, Investigation, Funding acquisition, Formal analysis, Data curation, Conceptualization.

Declaration of competing interest

The authors declare the following financial interests/personal relationships which may be considered as potential competing interests: Jose L. Simon reports financial support was provided by Agencia Estatal de Investigación, Spanish Government. Alba Peiro reports financial support was provided by Agencia Estatal de Investigación, Spanish Government. Luis E. Arlegui reports financial support was provided by Agencia Estatal de Investigación, Spanish Government.

Data availability

Data will be made available on request.

Acknowledgments

The research has been financed by project PID2019-108705-GB-I00 of the Agencia Estatal de Investigación (AEI/10.13039/501100011033) of the Spanish Government. This work is a contribution of the Geotransfer Research Group (E32_20R) funded by Gobierno de Aragón. A. Peiro has benefited from a FPU contract (FPU17/02470) of the Spanish Government. We thank C. Liesa, A. Luzón and L. Ezquerro, members of our research group on active faults in the Iberian Chain, for their help. We thank Luis Carlos Puertas from the National Geographic Institute (IGN, Spain) for his help to Fig. 3c presented in this work. We are also grateful for the collaboration provided by the Celadas Town Council for the installation of the IGN seismic station. We deeply acknowledge the suggestions by two anonymous reviewers that carefully read a previous version of the manuscript.

References

Aki, K., 1965. Maximum likelihood estimate of b in the formula logN = a-bM and its confidence limits. Bull. Earthq. Res. Inst. 43, 237–239.

Allmendinger, R.W., Cardozo, N.C., Fisher, D., 2013. Structural Geology Algorithms: Vectors & Tensors. Cambridge University Press, Cambridge.

Álvaro, M., Capote, R., Vegas, R., 1979. Un modelo de evolución geotectónica para la Cadena Celtibérica. Acta Geol. Hisp. 14, 172–177.

Anders, M.H., Schlische, R.W., 1994. Overlapping faults, intrabasin highs, and the growth of normal faults. J. Geol. 102, 165–179.

Arlegui, L.E., Simón, J.L., Lisle, R.J., Orife, T., 2005. Late Pliocene-Pleistocene stress field in the Teruel and Jiloca Grabens (eastern Spain): contribution of a new method of stress inversion. J. Struct. Geol. 27, 693–705.

Bawden, G.W., Michael, A.J., Kellogg, L.H., 1999. Birth of a fault: Connecting the Kern County and Walker Pass, California, earthquakes. Geology 27, 61–64.

Bonini, M., Corti, G., Delle Donne, D., Sani, F., Piccardi, L., Vannucci, G., Genco, R., Martelli, L., Ripepe, M., 2016. Seismic sources and stress transfer interaction among axial normal faults and external thrust fronts in the Northern Apennines (Italy): a working hypothesis based on the 1916–1920 time–space cluster of earthquakes. Tectonophysics 680, 67–89.

Bratt, S., Naggy, W., 1991. The LocSAT Program, Science Applications International Corporation (SAIC). San Diego, California.

Cabañas, L., Rivas-Medina, A., Martínez-Solares, J.M., Gaspar-Escribano, J.M., Benito, B., Antón, R., Ruiz-Barajas, S., 2015. Relationships between Mw and other earthquake size parameters in the Spanish IGN seismic catalog. Pure Appl. Geophys. 172, 2397–2410. https://doi.org/10.1007/s00024-014-1025-2.

Capote, R., Muñoz, J.A., Simón, J.L., Liesa, C.L., Arlegui, L.E., 2002. Alpine tectonics I: The alpine system north of the betic cordillera. In: Gibbons, W., Moreno, T. (Eds.), Geology of Spain. The Geological Society, London, pp. 367–400.

Cardozo, N., Allmendinger, R.W., 2013. Spherical projections with OSXStereonet. Comput. Geosci. 51, 193–205.

Childs, C., Watterson, J., Walsh, J.J., 1995. Fault overlap zones within developing normal fault systems. J. Geol. Soc. 152, 535–549. London.

Crider, J.G., Pollard, D.D., 1998. Fault linkage: three-dimensional mechanical interaction between echelon normal faults. J. Geophys. Res. 103, 675–692.

Diaz, J., Gallart, J., 2009. Crustal structure beneath the Iberian Peninsula and surrounding waters: a new compilation of deep seismic sounding results. Phys. Earth Planet. Inter. 173, 181–190.

Ezquerro, L., 2017. El sector norte de la cuenca neógena de Teruel: tectónica, clima y sedimentación. PhD thesis. Univ. Zaragoza. http://zaguan.unizar.es/record/77098#.

Ezquerro, L., Simón, J.L., Luzón, A., Liesa, C.L., 2020. Segmentation and increasing activity in the Neogene-Quaternary Teruel Basin rift (Spain) revealed by morphotectonic approach. J. Struct. Geol. 135, 104043.

Ferrarini, F., De Nardis, R., Brozzetti, F., Cirillo, D., Arrowsmith, J.R., Lavecchia, G., 2021. Multiple lines of evidence for a potentially seismogenic fault along the central-Apennine (Italy) active extensional belt–An unexpected outcome of the MW6. 5 Norcia 2016 Earthquake. Front. Earth Sci. 9, 642243.

Fossen, H., Rotevatn, A., 2016. Fault linkage and relay structures in extensional settings - a review. Earth Sci. Rev. 154, 14–28.

García-Mayordomo, J., Insua-Arévalo, J.M., Martínez-Díaz, J.J., Jiménez-Díaz, A., Martín-Banda, R., Martín-Alfageme, S., Álvarez-Gómez, J.A., Rodríguez-Peces, M., Pérez-López, R., Rodríguez-Pascua, M.A., et al., 2012. The Quaternary Active Faults Database of Iberia (QAFI v.2.0). J. Iber. Geol. 38, 285–302.

GFZ, German Research Centre for Geosciences, and GEMPA GmbH, 2008. The SeisComP seismological software package. GFZ Data Svc. https://doi.org/10.5880/GFZ.2.4.2020.003.

Godoy, A., Moissenet, E., Ramírez, J.I., Olivé, A., Aznar, J.M., Jerez, L., Aragonés, E., Aguilar, M.J., Ramírez Del Pozo, J., Leal, M.C., Adrover, R., Alberdi, M.T., Giner, J., Gutiérrez, M., Portero, J.M., Gabaldón, V., 1983a. Mapa Geológico de España 1: 50.000. Hoja 542 (Alfambra). Instituto Geológico y Minero de España, Madrid.

Godoy, A., Ramírez, J.I., Olivé, A., Moissenet, E., Aznar, J.M., Aragonés, E., Aguilar, M.J., Ramírez Del Pozo, J., Leal, M.C., Jerez Mir, L., Adrover, R., Goy, A., Comas, M.J., Alberdi, M.T., Giner, J., Gutiérrez Elorza, M., Portero, J.M., Gabaldón, V., 1983b. Mapa Geológico de España 1: 50.000. Hoja 567 (Teruel). Instituto Geológico y Minero de España, Madrid.

Gutenberg, B., Richter, C.F., 1944. Frequency of earthquakes in California. Bull. Seismol. Soc. Am. 34, 185–188.

Gutiérrez, F., Gracia, F.J., Gutiérrez, M., Lucha, P., Guerrero, J., Carbonel, D., Galve, J.P., 2012. A review on Quaternary tectonic and nontectonic faults in the central sector of the Iberian Chain, NE Spain. J. Iber. Geol. 38, 145–160.

Hernández, A., Ramírez, J.I., Olivé, A., Riba, O., Aragonés, E., Aguilar, M.J., Ramírez del Pozo, J., Leal, M.C., Giner, J., Gutiérrez, M., Goy, A., Comas, M.J., Gutiérrez, J.L., Portero, J.M., Gabaldón, V., 1983. Mapa Geológico de España 1: 50.000. In: hoja 566 (Cella). Instituto Geológico y Minero de España, Madrid.
Herraiz, M., De Vicente, G., Lindo-Naupari, R., Giner, J., Simón, J.L., González-Casado, J. M., Vadillo, O., Rodríguez-Pascua, M.A., Cicuéndez, J.L., Casas, A., Cabañas, L., Rincón, P., Cortés, A.L., Ramírez, M., Lucini, M., 2000. The recent (upper Miocene to Quaternary) and present tectonic stress distributions in the Iberian Peninsula. Tectonics 19, 762–786.
Irwin, G.R., 1957. Analysis of stresses and strains near the end of a crack transversing a plate. J. Appl. Mech. 24, 361–364.
Kennett, B.L.N., Engdahl, E.R., 1991. Traveltimes for global earthquake location and phase identification. Geophys. J. Int. 122, 429–465.
Koirala, B.P., Laporte, M., Bollinger, L., Batteux, D., Letort, J., Trilla, A.G., Wendling-Vzquez, N., Bhattarai, M., Subedi, S., Adhikari, L.B., 2023. Tectonic significance of the 2021 Lamjung, Nepal, mid-crustal seismic cluster. Earth Planets Space 75, 165.
Lafuente, P., 2011. Tectónica activa y paleosismicidad de la falla de Concud (Cordillera Ibérica central). PhD thesis.. Univ. Zaragoza.
Lafuente, P., Arlegui, L.E., Liesa, C.L., Simón, J.L., 2011a. Paleoseismological analysis of an intraplate extensional structure: the Concud fault (Iberian Chain, Eastern Spain). Int. J. Earth Sci. 100, 1713–1732.
Lafuente, P., Arlegui, L.E., Casado, I., Ezquerro, L., Liesa, C.L., Pueyo, O., Simón, J.L., 2011b. Geometría y cinemática de la zona de relevo entre las fallas neógeno-cuaternarias de Concud y Teruel (Cordillera Ibérica). Rev. Soc. Geol. Esp. 24, 109–125.
Lafuente, P., Arlegui, L.E., Liesa, C.L., Pueyo, O., Simón, J.L., 2014. Spatial and temporal variation of paleoseismic activity at an intraplate, historically quiescent structure: the Concud fault (Iberian Chain, Spain). Tectonophysics 632, 167–187.
Lai, K.Y., Chen, Y.G., Wu, Y.M., Avouac, J.P., Kuo, Y.T., Wang, Y., Chang, C.H., Lin, K.C., 2009. The 2005 Ilan earthquake doublet and seismic crisis in northeastern Taiwan: evidence for dyke intrusion associated with on-land propagation of the Okinawa Trough. Geophys. J. Int. 179, 678–686.
Liesa, C.L., Simón, J.L., 2009. Evolution of intraplate stress fields under multiple remote compressions: the case of the Iberian Chain (NE Spain). Tectonophysics 474, 144–159.
Liesa, C.L., Simón, J.L., Casas, A.M., 2018. La tectónica de inversión en una región intraplaca: La Cordillera Ibérica. Rev. Soc. Geol. Esp. 31, 23–50.
Liesa, C.L., Simon, J.L., Ezquerro, L., Arlegui, L.E., Luzón, A., 2019. Stress evolution and structural inheritance controlling an intracontinental extensional basin: the central-northern sector of the Neogene Teruel Basin. J. Struct. Geol. 118, 362–376.
Lieser, K., Grevemeyer, I., Lange, D., Flueh, E., Tilmann, F., Contreras-Reyes, E., 2014. Splay fault activity revealed by aftershocks of the 2010 Mw 8.8 Maule earthquake, Central Chile. Geology 42, 823–826.
Lomax, A., Virieux, J., Volant, P., Berge-Thierry, C., 2000. Probabilistic earthquake location in 3D and layered models. In: Thurber, C.H., Rabinowitz, N. (Eds.), Advances in Seismic Event Location. Springer, Netherlands, Dordrecht, pp. 101–134.
Mansfield, C., Cartwright, J., 2001. Fault growth by linkage: observations and implications from analogue models. J. Struct. Geol. 23, 745–763.
Mezcua, J., Martínez Solares, J.M., 1983. Sismicidad en el área Ibero-Magrebí. Publicación Técnica no. 203. Instituto Geográfico Nacional, Madrid.
Mignan, A., Woessner, J., 2012. Estimating the magnitude of completeness for earthquake catalogs. In: CORSSA (Community Online Resource for Statistical Seismicity Analysis), pp. 1–45.
Olivé, A., Hernández, A., Moissenet, E., Pardo, G., Villena, J., Gutiérrez, M., Puigdefábregas, C., Giner, J., Aguilar, M.J., Leal, M.C., Goy, A., Comas, M.J., Adrover, R., Portero, J.M., Gabaldón, V., 1983. Mapa Geológico de España 1: 50.000. In: Hoja 516 (Monreal del Campo). Instituto Geológico y Minero de España, Madrid.
Peacock, D.C.P., 2002. Propagation, interaction and linkage in normal fault systems. Earth Sci. Rev. 58, 121–142.
Peacock, D.C.P., Sanderson, D.J., 1991. Displacements, segment linkage and relay ramps in normal fault zones. J. Struct. Geol. 13, 721–733.
Peacock, D.C.P., Sanderson, D.J., 1994. Geometry and development of relay ramps in normal fault systems. Bull. Am. Assoc. Pet. Geol. 78, 147–165.
Peiro, A., Simón, J.L., Liesa, C.L., 2017. New evidence of recent fracturing at the relay zone between the Concud and Teruel faults (eastern Iberian Chain). Geogaceta 62, 31–34.
Peiro, A., Simón, J.L., Román-Berdiel, T., 2020. Fault relay zones evolving through distributed longitudinal fractures: the case of the Teruel graben system (Iberian Chain, Spain). J. Struct. Geol. 131, 103942.
Peiro, A., Simón, J.L., Arlegui, L.E., Ezquerro, L., García-Lacosta, A.I., Lamelas, M.T., Liesa, L., Luzón, A., Martín-Bello, L., Pueyo-Anchuela, Ó., Russo, N., 2022. Hanging-wall deformation at the active Sierra Palomera extensional fault (Jiloca basin, Spain) from structural, morphotectonic, geophysical and trench study. Tectonophysics 828, 229274.
Ramírez, J.I., Olivé, A., Moissenet, E., Aragonés, E., Ramírez, J., Leal, M.C., Aguilar, M.J., Adrover, R., Giner, J., Gutiérrez, J.C., Goy, A., Comas, M.J., Portero, J.M., Gabaldón, V., 1983. Mapa Geológico de España 1: 50.000. In: Hoja 541 (Santa Eulalia). Instituto Geológico y Minero de España, Madrid.
Ramsay, J.G., Huber, M.I., 1987. The Techniques of Modern Structural Geology, 2. Folds and Fractures. Academic Press, London, pp. 309–700.
Roca, E., Guimerà, J., 1992. The Neogene structure of the eastern Iberian margin: structural constraints on the crustal evolution of the Valencia trough (western Mediterranean). Tectonophysics 203, 203–218.
Rubio, J.C., Simón, J.L., 2007. Tectonic subsidence vs. Erosional lowering in a controversial intramontane depression: the Jiloca Basin (Iberian Chain, Spain). Geol. Mag. 144, 1–15.
Rydelek, P.A., y Sacks, I.S., 1989. Testing the completeness of earthquake catalogues and the hypothesis of self-similarity. Nature 337 (6204), 251–253.
Schlische, R.W., 1992. Structural and stratigraphic development of the Newark extensional basin, eastern North America; implications for the growth of the basin and its bounding structures: Geol. Soc. America Bull. 104, 1246–1263.
Simón, J.L., 1982. Compresión y Distensión Alpinas en la Cadena Ibérica Oriental. PhD thesis.. Universidad de Zaragoza. Instituto de Estudios Turolenses, Teruel.
Simón, J.L., 1983. Tectónica y Neotectónica del Sistema de Fosas de Teruel. Teruel, 69, pp. 21–97.
Simón, J.L., 1989. Late cenozoic stress field and fracturing in the iberian Chain and Ebro basin (Spain). J. Struct. Geol. 11, 285–294.
Simón, J.L., Arlegui, L., Lafuente, P., Liesa, C.L., 2012. Active extensional faults in the central-eastern Iberian Chain, Spain. J. Iber. Geol. 38, 127–144.
Simón, J.L., Arlegui, L.E., Ezquerro, L., Lafuente, P., Liesa, C.L., Luzón, A., 2016. Enhaced paleoseismic succession at the Concud Fault (Iberian Chain, Spain): new insights for seismic hazard assessment. Nat. Hazards 80, 1967–1993.
Simón, J.L., Arlegui, L.E., Ezquerro, L., Lafuente, P., Liesa, C.L., Luzón, A., 2017. Structure and paleoseismology of the Teruel fault: dynamic interaction and strain partitioning with the Concud fault (eastern Iberian Chain, Spain). J. Struct. Geol. 103, 100–119.
Simón, J.L., Ezquerro, L., Arlegui, L.E., Liesa, C.L., Luzón, A., Medialdea, A., García, A., Zarazaga, D., 2019. Role of transverse structures in paleoseismicity and drainage rearrangement in rift systems: the case of the Valdecebro fault zone (Teruel graben, eastern Spain). Int. J. Earth Sci. 108, 1429–1449.
Simón, J.L., Peiro, A., Arlegui, L.E., Ezquerro, L., García-Lacosta, A.I., Lafuente, P., Liesa, C.L., Luzón, A., Martín-Bello, L., Pueyo, O., Soriano, M.A., 2022. Actividad plio-cuaternaria de fallas en el sistema extensional Teruel-Jiloca-Calatayud (Cordillera Ibérica central). In: Resúmenes IV Reunión Ibérica sobre Fallas Activas y Paleosismología (Iberfault-22). Universidad de Zaragoza, Teruel, pp. 27–30.
Simón-Porcar, G., Simón, J.L., Liesa, C.L., 2019. La cuenca neógena extensional de El Pobo (Teruel, Cordillera Ibérica): sedimentología, estructura y relación con la evolución del relieve. Revista de la Sociedad Geológica España 32, 17–42.
Stein, S., Wysession, M., 2003. An Introduction to Seismology, Earthquakes, and Earth Structure. Blackwell, Malden, p. 498.
Tarantola, A., Valette, B., 1982. Generalized nonlinear inverse problems solved using the least squares criterion. Rev. Geophys. 20, 219–232.
Trudgill, B., Cartwright, J., 1994. Relay-ramp forms and normal-fault linkages, canyonlands national park. Utah. Bull. Geol. Soc. Am. 106, 1143–1157.
Turcotte, D.L., 1986. A fractal model for crustal deformation. Tectonophysics 132, 261–269.
Walsh, J.J., Watterson, J., Bailey, W.R., Childs, C., 1999. Fault relays, bends and branch-lines. J. Struct. Geol. 21, 1019–1026.
Wiemer, S., 2001. A software package to analyze seismicity: ZMAP. Seismol. Res. Lett. 72 (3), 373–382.
Wiemer, S., Wyss, M., 2000. Minimum magnitude of completeness in earthquake catalogs: examples from Alaska, the western US and Japan. Bull. Seismol. Soc. Am. 90, 859–869.
Willemse, E.J.M., 1997. Segmented normal faults: correspondence between three-dimensional mechanical models and field data. J. Geophys. Res. 1902, 675–692.